Supporting Information

Exploring optical management and efficiency limit of luminescent solar concentrators based on advanced luminophores

Qi Nie[1], Wenqing Li[1], Kuilin Li[1] and Xiao Luo[1]*

[1]School of Optoelectronic Science and Engineering, University of Electronic Science and Technology of China (UESTC), Chengdu 610054, PR China

*To whom correspondence and requests for materials should be addressed: luox@uestc.edu.cn.

Monte Carlo simulation

Monte Carlo (MC) simulation is a very effective way to explore the performance characteristics of LSCs, as the principle of LSCs does not involve phase-dependent wave effects such as interference and diffraction. MC simulation is actually a representation of a statistical law, and when enough events are simulated, it will exhibit physical laws close to the actual one. Firstly, each randomly generated photon will carry information about wavelength and coordinates. The number of photons will reach 10^6 to have a proper statistical averaging. And all the energy of sunlight is considered to be uniformly incident on the surface of the LSC. When each photon is randomly generated, it undergoes scattering or absorption. If one photon is absorbed by the luminophores, then the photogenerated exciton can either undergo nonradiative recombination or decay radiatively producing a photon, which is based on the PLQY. And the information about wavelength and direction cosines of the photon will be updated. According to the direction cosines of the remitted photon, whether the photon will undergo internal total reflection will be determined. When the photon reaches at the surfaces of LSC, whether the photon enters the internal total reflection or exits from the top and bottom surfaces will be determined.

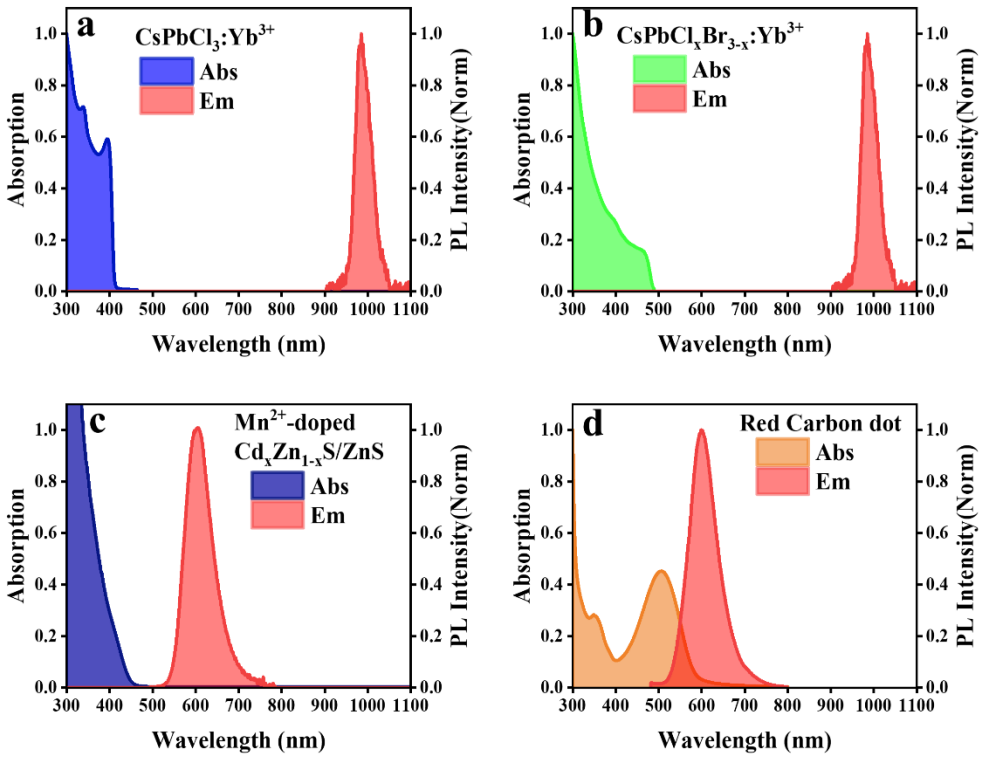

Figure S1. (a) The absorption and PL spectral for $CsPbCl_3:Yb^{3+}$ NCs. (b) The absorption and PL spectral for $CsPbCl_xBr_{3-x}:Yb^{3+}$ NCs. (c) The absorption and PL spectral for Mn^{2+}-doped $Cd_xZn_{1-x}S/ZnS$ QDs. (d) The absorption and PL spectral for red CDs.

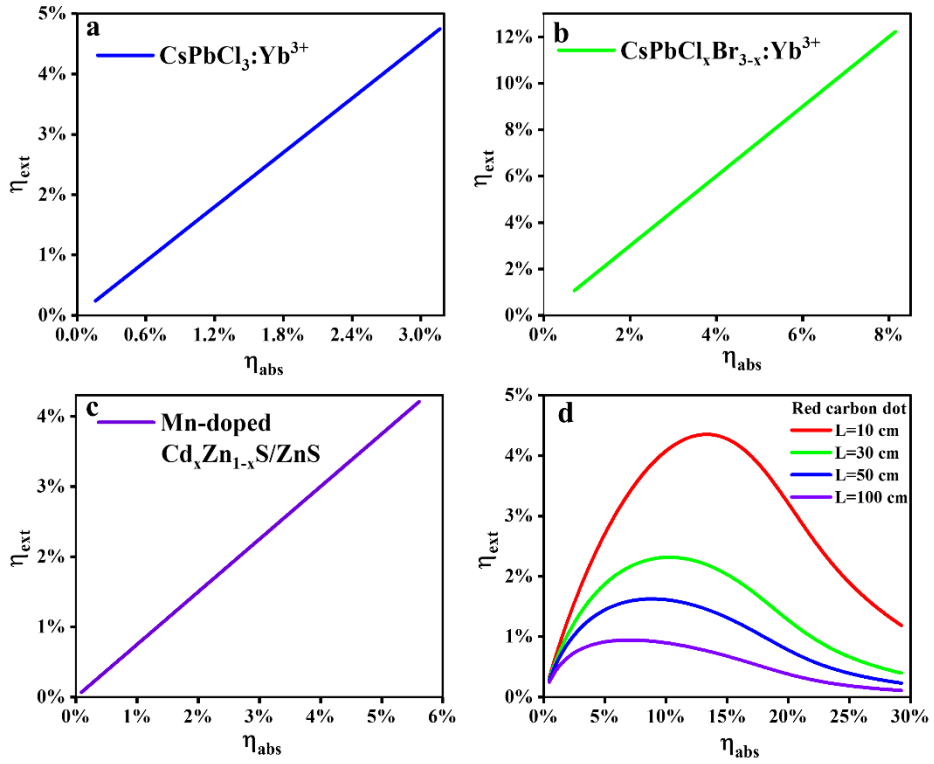

Figure S2. (a) Extrapolated η_{abs}-dependent η_{ext} for $CsPbCl_3:Yb^{3+}$ NCs. (b) Extrapolated η_{abs}-dependent η_{ext} for $CsPbCl_xBr_{3-x}:Yb^{3+}$ NCs. (c) Extrapolated η_{abs}-dependent η_{ext} for Mn^{2+}-doped $Cd_xZn_{1-x}S/ZnS$ QDs. (d) Extrapolated η_{abs}-dependent η_{ext} for red CDs. The red, green, blue and purple lines represented the length of LSCs to be 10 cm, 30 cm, 50 cm and 100 cm respectively.

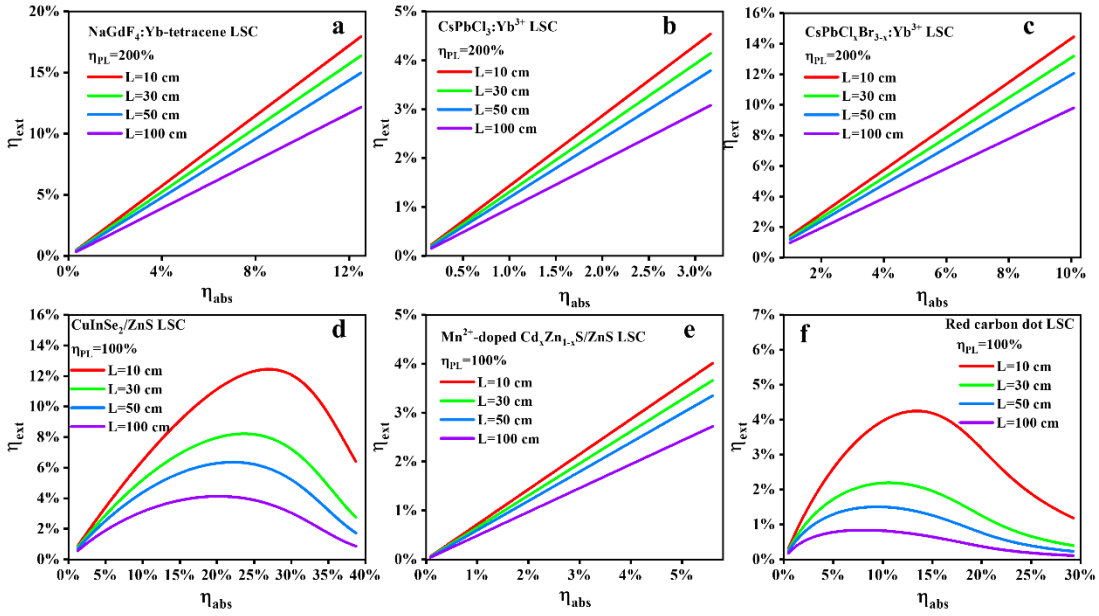

Figure S3. Extrapolated η_{abs}-dependent η_{ext} for $NaGdF_4:Yb$-tetracene NCs (a), $CsPbCl_3:Yb^{3+}$ NCs (b), $CsPbCl_xBr_{3-x}:Yb^{3+}$ NCs (c), $CuInSe_2/ZnS$ QDs (d), Mn^{2+}-doped $Cd_xZn_{1-x}S/ZnS$ QDs (e) and red CDs (f) under the situation that considering the scattering factor to be 0.012 cm^{-1} under ideal PLQY. The red, green, blue and purple lines represented the length of LSCs to be 10 cm, 30 cm, 50 cm and 100 cm respectively.

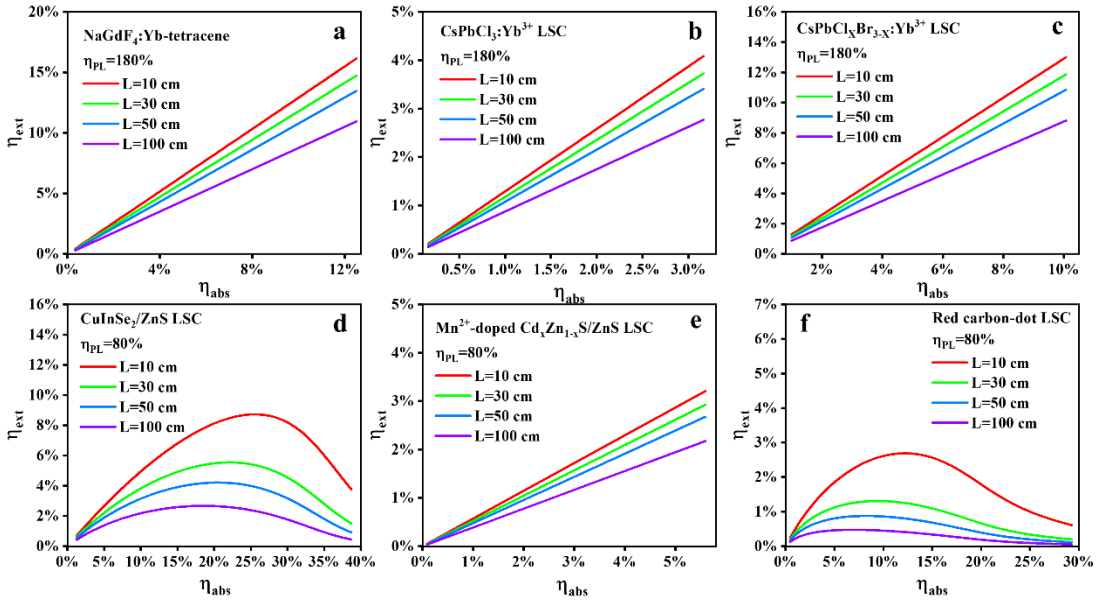

Figure S4. Extrapolated η_{abs}-dependent η_{ext} for $NaGdF_4$:Yb-tetracene NCs (a), $CsPbCl_3:Yb^{3+}$ NCs (b), $CsPbCl_xBr_{3-x}:Yb^{3+}$ NCs (c), $CuInSe_2$/ZnS QDs (d), Mn^{2+}-doped $Cd_xZn_{1-x}S$/ZnS QDs (e) and red CDs (f) under the situation that considering the scattering factor to be 0.012 cm^{-1} under unideal PLQY. The red, green, blue and purple lines represented the length of LSCs to be 10 cm, 30 cm, 50 cm and 100 cm respectively.

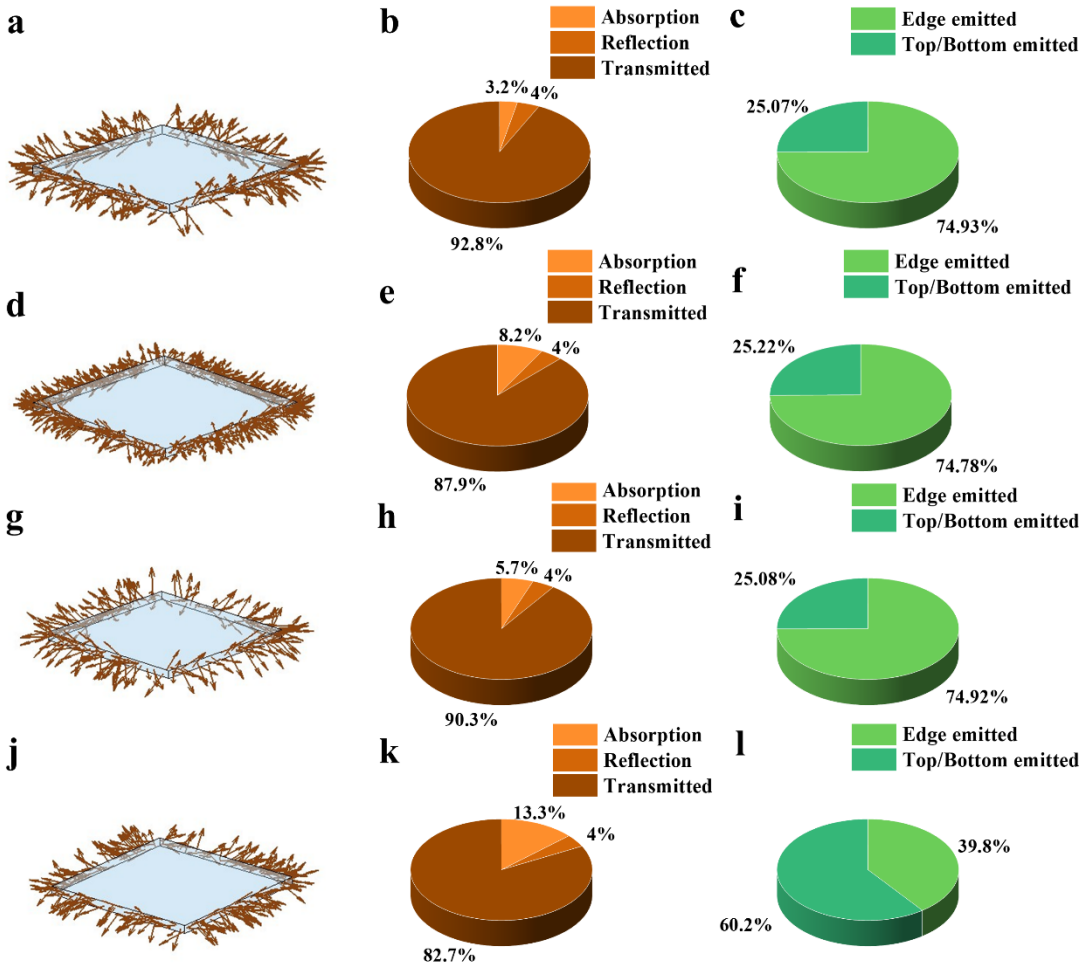

Figure S5. The Monte Carlo ray-tracing simulations for $CsPbCl_3:Yb^{3+}$ NCs based LSCs, $CsPbCl_xBr_{3-x}:Yb^{3+}$ based LSCs, Mn^{2+}-doped $Cd_xZn_{1-x}S$/ZnS QDs based LSCs and red CDs based LSCs with the dimension of 10×10×0.5 cm^3 under ideal situation. (a) the light simulation diagram of $CsPbCl_3:Yb^{3+}$ NCs based LSCs. (b) the statistical diagram of incident photons of $CsPbCl_3:Yb^{3+}$ NCs based LSCs. (c) the statistical diagram of emitted photons of $CsPbCl_3:Yb^{3+}$ NCs based LSCs. (d) the light simulation diagram of $CsPbCl_xBr_{3-x}:Yb^{3+}$ NCs based LSCs. (e) the statistical diagram of incident photons of $CsPbCl_xBr_{3-x}:Yb^{3+}$ NCs based LSCs. (f) the statistical diagram of emitted photons of $CsPbCl_xBr_{3-x\ 3}:Yb^{3+}$ NCs based LSCs. (g) the light simulation diagram of Mn^{2+}-doped $Cd_xZn_{1-x}S$/ZnS QDs based LSCs. (h) the statistical diagram of incident photons of Mn^{2+}-doped $Cd_xZn_{1-x}S$/ZnS QDs based LSCs. (i) the statistical diagram of emitted photons of Mn^{2+}-doped $Cd_xZn_{1-x}S$/ZnS QDs based LSCs. (j) the light simulation

diagram of red CDs based LSCs. (k) the statistical diagram of incident photons of red CDs based LSCs. (l) the statistical diagram of emitted photons of red CDs based LSCs.

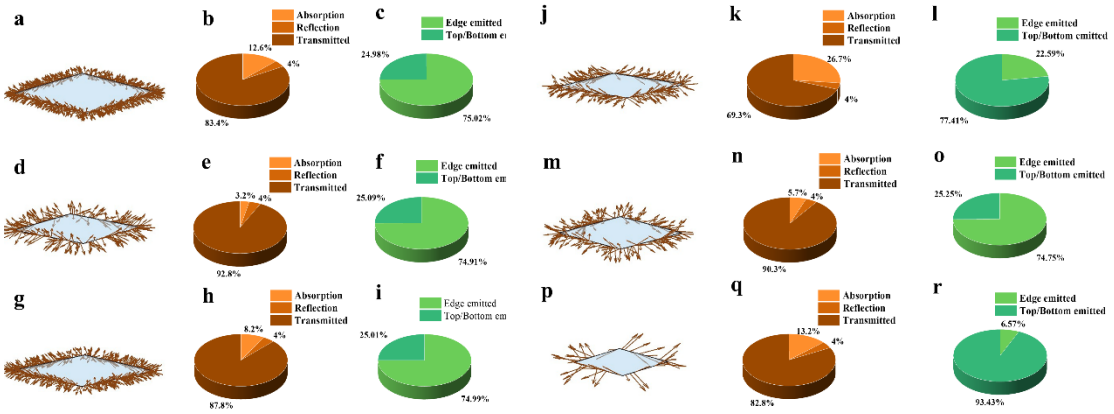

Figure S6. The Monte Carlo ray-tracing simulations for $NaGdF_4$:Yb-tetracene NCs based LSCs, $CsPbCl_3:Yb^{3+}$ NCs based LSCs, $CsPbCl_xBr_{3-x}:Yb^{3+}$ based LSCs, $CuInSe_2$/ZnS QDs based LSCs, Mn^{2+}-doped $Cd_xZn_{1-x}S$/ZnS QDs based LSCs and red CDs based LSCs with the dimension of 100×100×0.5 cm^3 under ideal situation. (a) the light simulation diagram of $NaGdF_4$:Yb-tetracene NCs based LSCs. (b) the statistical diagram of incident photons of $NaGdF_4$:Yb-tetracene NCs based LSCs. (c) the statistical diagram of emitted photons of $NaGdF_4$:Yb-tetracene NCs based LSCs. (d) the light simulation diagram of $CsPbCl_3:Yb^{3+}$ NCs based LSCs. (e) the statistical diagram of incident photons of $CsPbCl_3:Yb^{3+}$ NCs based LSCs. (f) the statistical diagram of emitted photons of $CsPbCl_3:Yb^{3+}$ NCs based LSCs. (g) the light simulation diagram of $CsPbCl_xBr_{3-x}:Yb^{3+}$ NCs based LSCs. (h) the statistical diagram of incident photons of $CsPbCl_xBr_{3-x}:Yb^{3+}$ NCs based LSCs. (i) the statistical diagram of emitted photons of $CsPbCl_xBr_{3-x}:Yb^{3+}$ NCs based LSCs. (j) the light simulation diagram of $CuInSe_2$/ZnS QDs based LSCs. (k) the statistical diagram of incident photons of $CuInSe_2$/ZnS QDs based LSCs. (l) the statistical diagram of emitted photons of $CuInSe_2$/ZnS QDs based LSCs. (m) the light simulation diagram of Mn^{2+}-doped $Cd_xZn_{1-x}S$/ZnS QDs based LSCs. (n) the statistical diagram of incident photons of Mn^{2+}-doped $Cd_xZn_{1-x}S$/ZnS QDs based LSCs. (o) the statistical diagram of emitted photons of Mn^{2+}-doped $Cd_xZn_{1-x}S$/ZnS QDs based LSCs. (p) the light simulation diagram of red CDs based LSCs. (q) the statistical diagram of incident photons of red CDs based LSCs. (r) the statistical diagram of emitted photons of red CDs based LSCs.

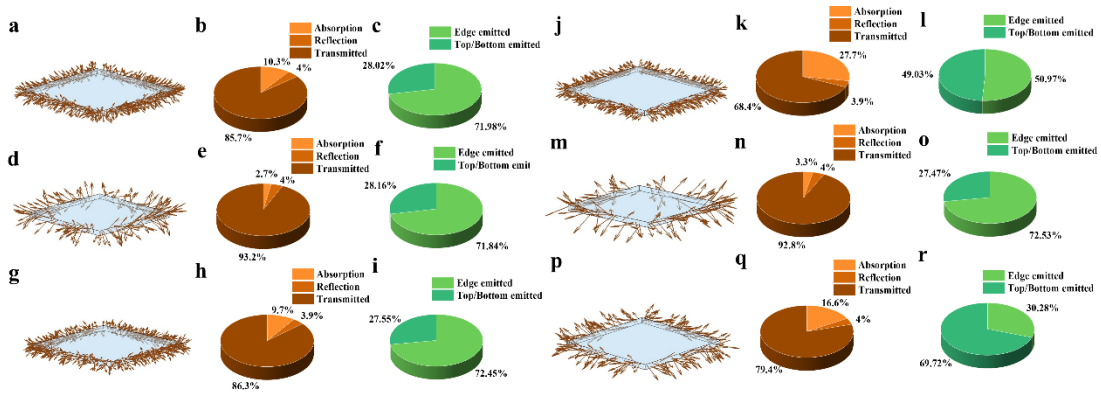

Figure S7. The Monte Carlo ray-tracing simulations for $NaGdF_4$:Yb-tetracene NCs based LSCs, $CsPbCl_3$:Yb^{3+} NCs based LSCs, $CsPbCl_xBr_{3-x}$:Yb^{3+} based LSCs, $CuInSe_2$/ZnS QDs based LSCs, Mn^{2+}-doped $Cd_xZn_{1-x}S$/ZnS QDs based LSCs and red CDs based LSCs with the dimension of 10×10×0.5 cm^3 under ideal PLQY and scattering factor of 0.012 cm^{-1}. (a) the light simulation diagram of $NaGdF_4$:Yb-tetracene NCs based LSCs. (b) the statistical diagram of incident photons of $NaGdF_4$:Yb-tetracene NCs based LSCs. (c) the statistical diagram of emitted photons of $NaGdF_4$:Yb-tetracene NCs based LSCs. (d) the light simulation diagram of $CsPbCl_3$:Yb^{3+} NCs based LSCs. (e) the statistical diagram of incident photons of $CsPbCl_3$:Yb^{3+} NCs based LSCs. (f) the statistical diagram of emitted photons of $CsPbCl_3$:Yb^{3+} NCs based LSCs. (g) the light simulation diagram of $CsPbCl_xBr_{3-x}$:Yb^{3+} NCs based LSCs. (h) the statistical diagram of incident photons of $CsPbCl_xBr_{3-x}$:Yb^{3+} NCs based LSCs. (i) the statistical diagram of emitted photons of $CsPbCl_xBr_{3-x}$:Yb^{3+} NCs based LSCs. (j) the light simulation diagram of $CuInSe_2$/ZnS QDs based LSCs. (k) the statistical diagram of incident photons of $CuInSe_2$/ZnS QDs based LSCs. (l) the statistical diagram of emitted photons of $CuInSe_2$/ZnS QDs based LSCs. (m) the light simulation diagram of Mn^{2+}-doped $Cd_xZn_{1-x}S$/ZnS QDs based LSCs. (n) the statistical diagram of incident photons of Mn^{2+}-doped $Cd_xZn_{1-x}S$/ZnS QDs based LSCs. (o) the statistical diagram of emitted photons of Mn^{2+}-doped $Cd_xZn_{1-x}S$/ZnS QDs based LSCs. (p) the light simulation diagram of red CDs based LSCs. (q) the statistical diagram of incident photons of red CDs based LSCs. (r) the statistical diagram of emitted photons of red CDs based LSCs.

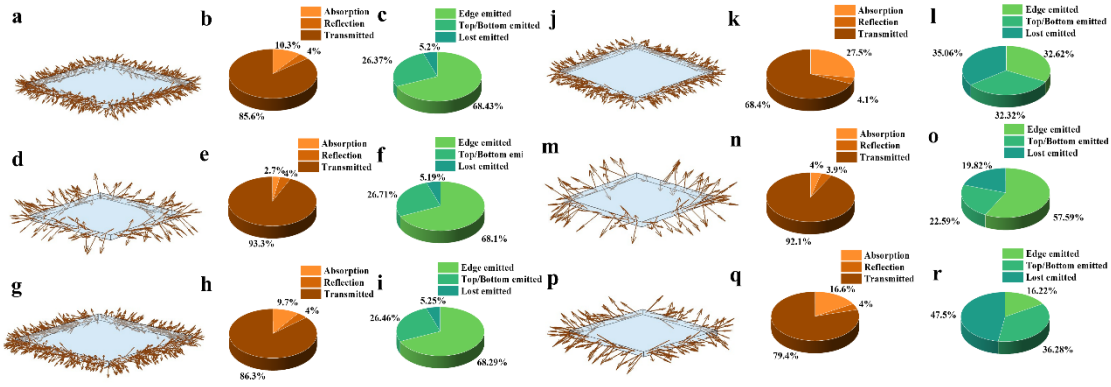

Figure S8. The Monte Carlo ray-tracing simulations for $NaGdF_4$:Yb-tetracene NCs based LSCs, $CsPbCl_3$:Yb^{3+} NCs based LSCs, $CsPbCl_xBr_{3-x}$:Yb^{3+} based LSCs, $CuInSe_2$/ZnS QDs based LSCs, Mn^{2+}-doped $Cd_xZn_{1-x}S$/ZnS QDs based LSCs and red CDs based LSCs with the dimension of 10×10×0.5 cm^3 under unideal PLQY and scattering factor of 0.012 cm^{-1}.. (a) the light simulation diagram of $NaGdF_4$:Yb-tetracene NCs based LSCs. (b) the statistical diagram of incident photons of $NaGdF_4$:Yb-tetracene NCs based LSCs. (c) the statistical diagram of emitted photons of $NaGdF_4$:Yb-tetracene NCs based LSCs. (d) the light simulation diagram of $CsPbCl_3$:Yb^{3+} NCs based LSCs. (e) the statistical diagram of incident photons of $CsPbCl_3$:Yb^{3+} NCs based LSCs. (f) the statistical diagram of emitted photons of $CsPbCl_3$:Yb^{3+} NCs based LSCs. (g) the light simulation diagram of $CsPbCl_xBr_{3-x}$:Yb^{3+} NCs based LSCs. (h) the statistical diagram of incident photons of $CsPbCl_xBr_{3-x}$:Yb^{3+} NCs based LSCs. (i) the statistical diagram of emitted photons of $CsPbCl_xBr_{3-x}$:Yb^{3+} NCs based LSCs. (j) the light simulation diagram of $CuInSe_2$/ZnS QDs based LSCs. (k) the statistical diagram of incident photons of $CuInSe_2$/ZnS QDs based LSCs. (l) the statistical diagram of emitted photons of $CuInSe_2$/ZnS QDs based LSCs. (m) the light simulation diagram of Mn^{2+}-doped $Cd_xZn_{1-x}S$/ZnS QDs based LSCs. (n) the statistical diagram of incident photons of Mn^{2+}-doped $Cd_xZn_{1-x}S$/ZnS QDs based LSCs. (o) the statistical diagram of emitted photons of Mn^{2+}-doped $Cd_xZn_{1-x}S$/ZnS QDs based LSCs. (p) the light simulation diagram of red CDs based LSCs. (q) the statistical diagram of incident photons of red CDs based LSCs. (r) the statistical diagram of emitted photons of red CDs based LSCs.

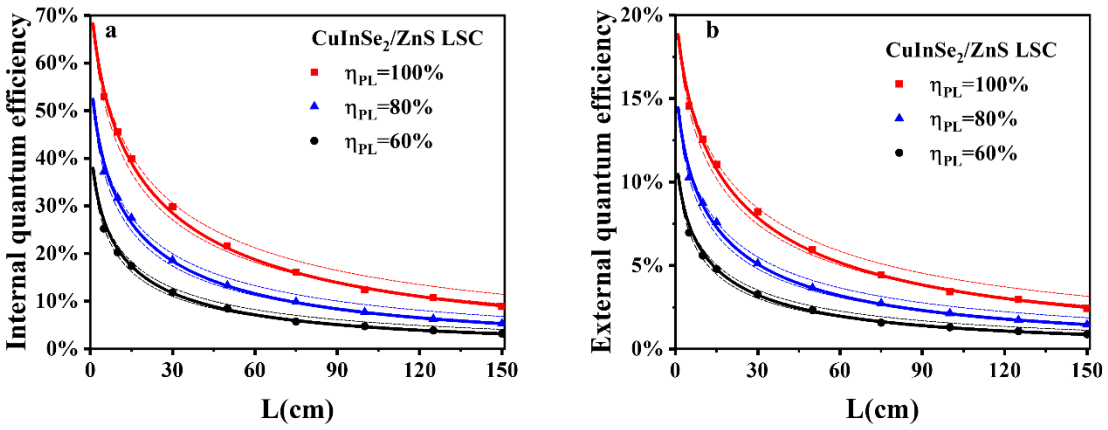

Figure S9. The Monte Carlo ray-tracing simulations of the L-dependent η_{int} (a) and η_{ext} (b) of $CuInSe_2$/ZnS QDs based LSCs with different η_{PL} under the situation that considering the scattering factor to be 0.012 cm^{-1}.

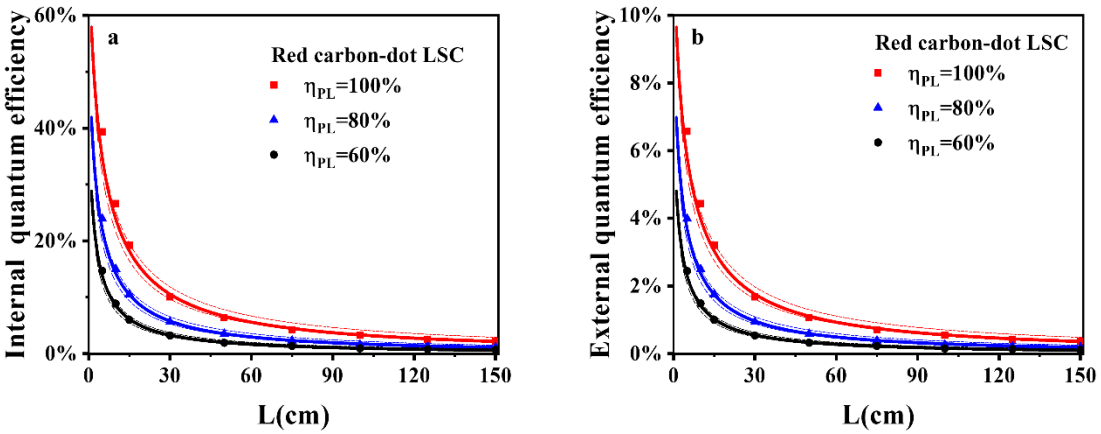

Figure S10. The Monte Carlo ray-tracing simulations of the L-dependent η_{int} (a) and η_{ext} (b) of red CDs based LSCs with different η_{PL} under the situation that considering the scattering factor to be 0.012 cm^{-1}.

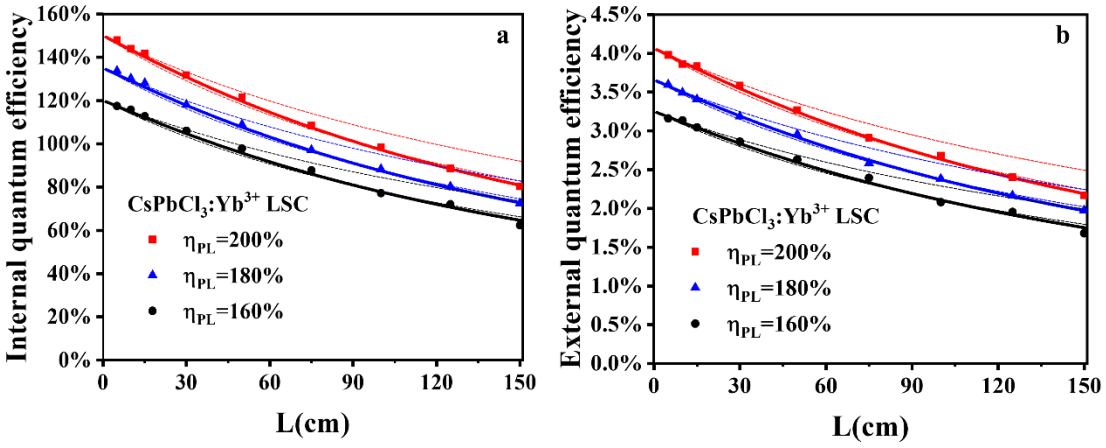

Figure S11. The Monte Carlo ray-tracing simulations of the L-dependent η_{int} (a) and η_{ext} (b) of $CsPbCl_3:Yb^{3+}$ NCs based LSCs with different η_{PL} under the situation that considering the scattering factor to be 0.012 cm^{-1}.

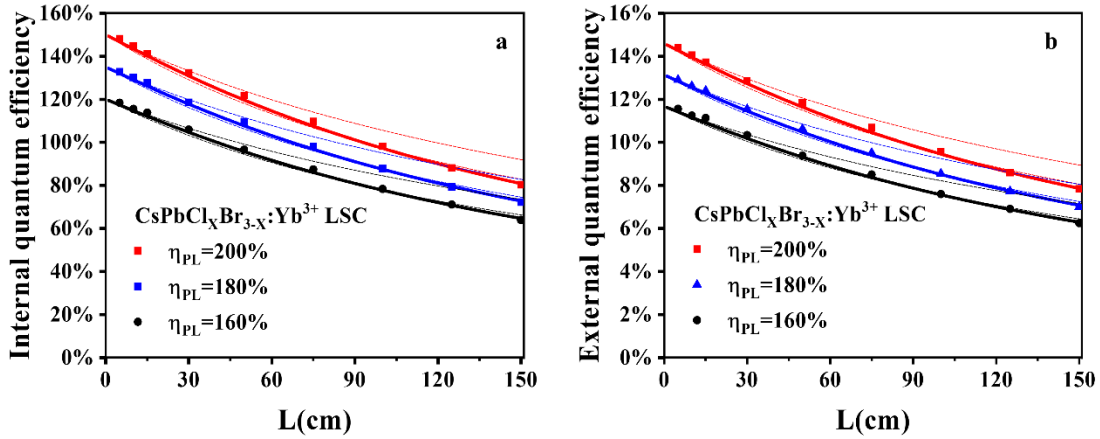

Figure S12. The Monte Carlo ray-tracing simulations of the L-dependent η_{int} (a) and η_{ext} (b) of $CsPbCl_xBr_{3-x}:Yb^{3+}$ NCs based LSCs with different η_{PL} under the situation that considering the scattering factor to be 0.012 cm^{-1}.

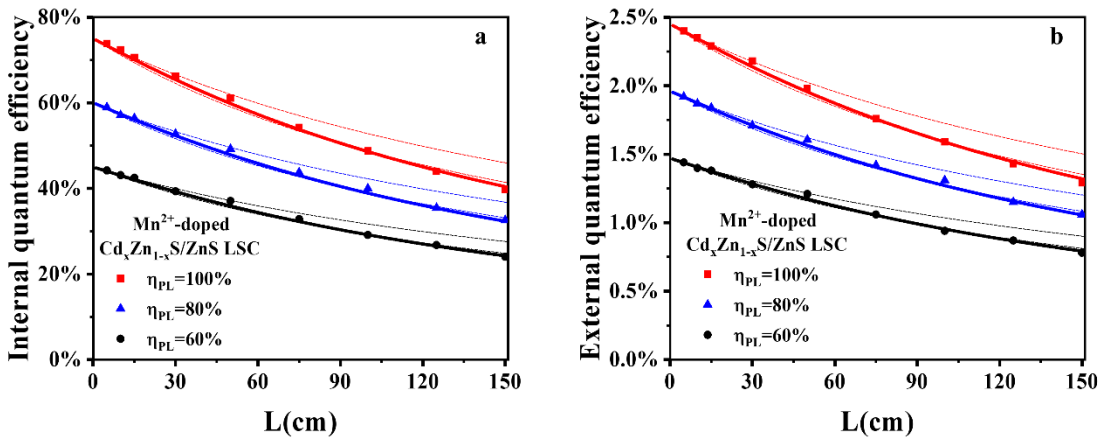

Figure S13. The Monte Carlo ray-tracing simulations of the L-dependent η_{int} (a) and η_{ext} (b) of Mn^{2+}-doped $Cd_xZn_{1-x}S/ZnS$ QDs based LSCs with different η_{PL} under the situation that considering the scattering factor to be 0.012 cm^{-1}.

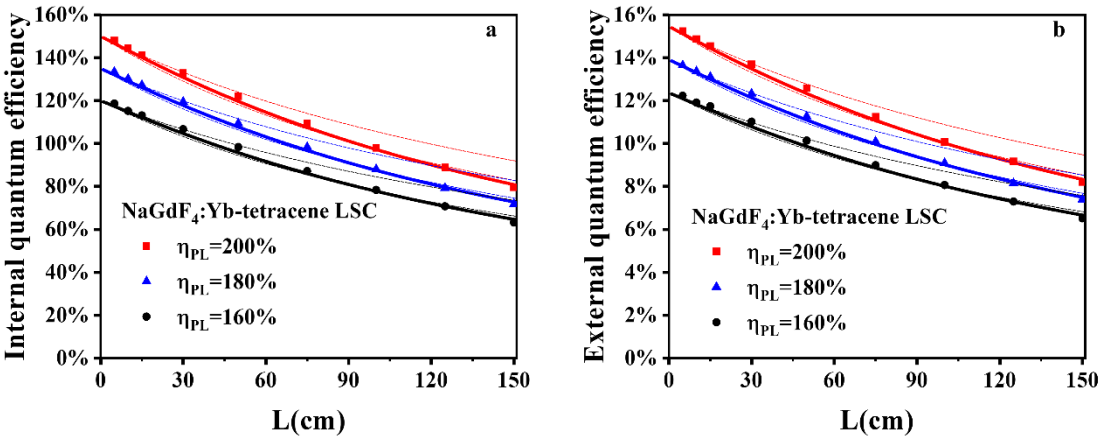

Figure S14. The Monte Carlo ray-tracing simulations of the L-dependent η_{int} (a) and η_{ext} (b) of $NaGdF_4$:Yb-tetracene NCs based LSCs with different η_{PL} under the situation that considering the scattering factor to be 0.012 cm^{-1}.

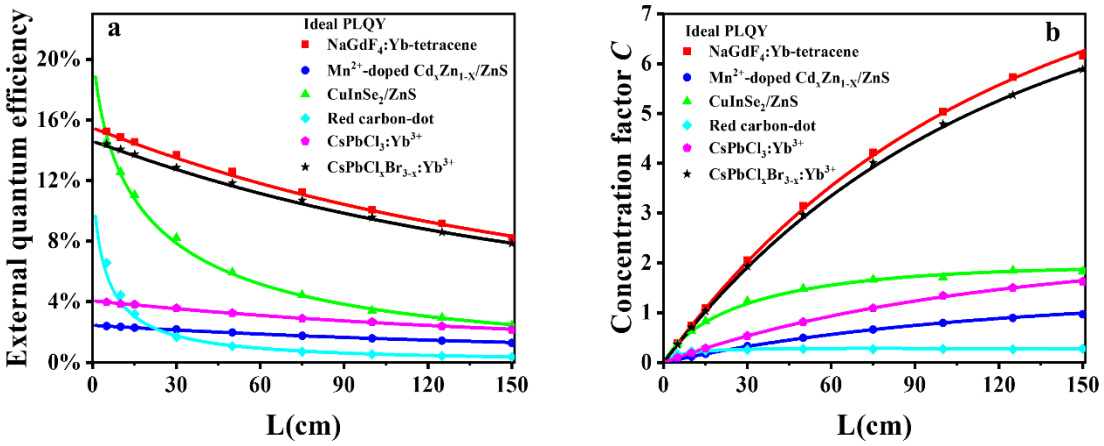

Figure S15. The Monte Carlo ray-tracing simulations of size-dependent η_{ext} under ideal situation (a) and concentration factor C (b) for $NaGdF_4$:Yb-tetracene NCs (red curve and dots), $CsPbCl_3:Yb^{3+}$ NCs (purple curve and dots), $CsPbCl_xBr_{3-x}:Yb^{3+}$ NCs (black curve and dots), $CuInSe_2$/ZnS QDs (green curve and dots), Mn^{2+}-doped $Cd_xZn_{1-x}S$/ZnS QDs (blue curve and dots) and red CDs (cyan curve and dots).

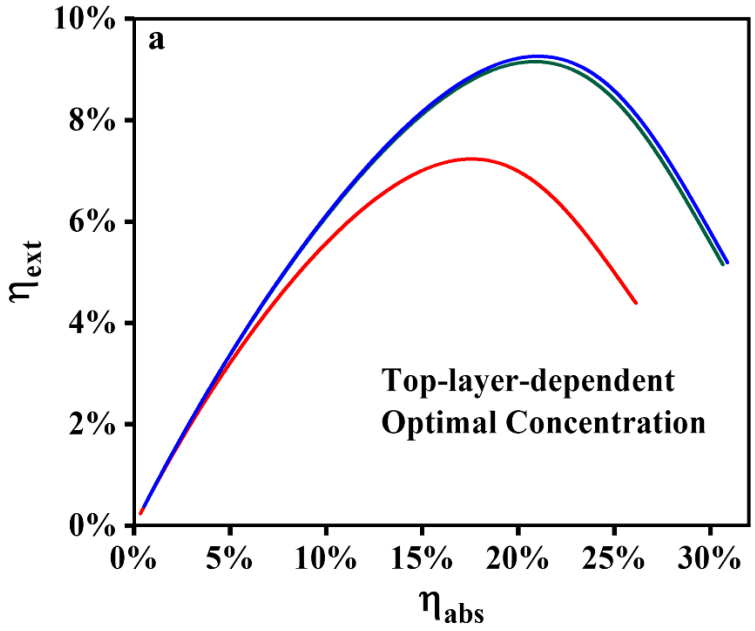

Figure S16. The curves of η_{abs}-dependent η_{ext} of $CuInSe_2$/ZnS QDs based LSCs using different top layer luminophores (red curves represented the $NaGdF_4$:Yb-tetracene NCs, green curves represented the $CuInSe_2$/ZnS QDs and blue curves represented the Mn^{2+}-doped $Cd_xZn_{1-x}S$/ZnS QDs).

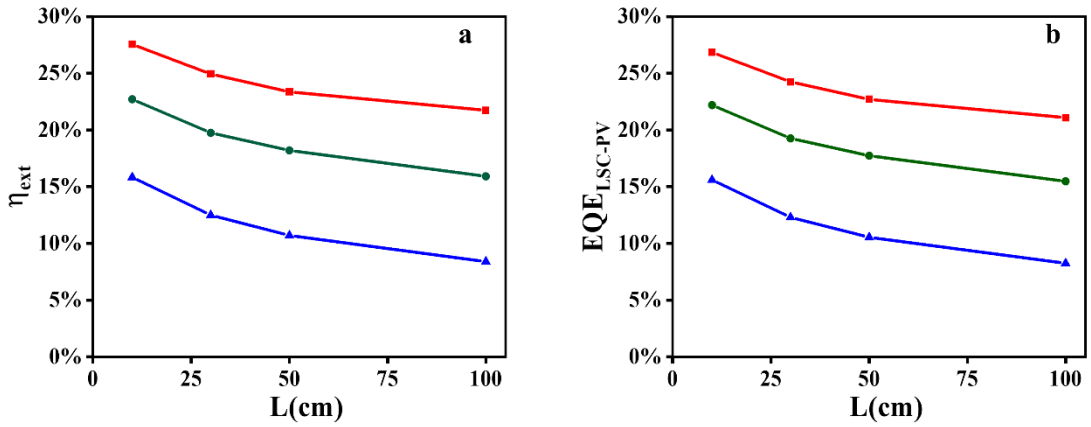

Figure S17. the Monte Carlo ray-tracing simulations of η_{ext} (a) and EQE_{LSC-PV} (b) of tandem LSC–PV systems for different top layer luminophores under ideal situation (red curves represented the $NaGdF_4$:Yb-tetracene NCs, green curves represented the $CuInSe_2$/ZnS QDs and blue curves represented the Mn^{2+}-doped $Cd_xZn_{1-x}S$/ZnS QDs) while using the $CuInSe_2$/ZnS QDs as the bottom layer luminophores.